Surface Oxidation of Single-walled-carbon-nanotubes with Enhanced Oxygen Electroreduction Activity and Selectivity①

CUI Ya-Qi[a, b] XU Jiao-Xing[a, b②]
WANG Mei-Lin[a, b] GUAN Lun-Hui[a, b②]

[a] (*College of Chemistry and Materials Science, Fujian Normal University, Fuzhou* 350007, *China*)

[b] (*CAS Key Laboratory of Design and Assembly of Functional Nanostructures, Fujian Provincial Key Laboratory of Nanomaterials, Fujian Institute of Research on the Structure of Matter, Chinese Academy of Sciences, Fuzhou* 350108, *China*)

ABSTRACT Electrochemical oxygen reduction reaction (ORR) with 2-electron process is an alternative for decentralized H_2O_2 production, but it remains high challenging to develop highly active and selective catalysts for this process. In this work, we present a selective and efficient nonprecious electrocatalyst, prepared through an easily scalable mild oxidation of single-walled carbon nanotubes (SWNTs) with different oxidative acids including sulfur acid, nitride acid and mixed sulfuric/nitric acids, respectively. The high-degree oxidized SWNTs treated by mixed acids exhibit the highest activity and selectivity of electroreduction of oxygen to synthesize H_2O_2 at low overpotential in alkaline and neutral media. Spectroscopic characterizations suggested that the C–O is vital for catalyzing 2-electron ORR, providing an insightful understanding of defected carbon surface as the active catalytic sites for 2-electron ORR.

Keywords: electrocatalysts, hydrogen peroxide production, oxygen reduction reaction;
DOI: 10.14102/j.cnki.0254–5861.2011–3157

1 INTRODUCTION

Hydrogen peroxide (H_2O_2) is an environmentally friendly chemical widely used in pulp, bleaching and wastewater treatment[1-3]. The anthraquinone method is the traditional industrial process for large scaled production of hydrogen peroxide, but it involves exorbitant infrastructures and sequential complicated distillation and purifications[4]. Free from these limits, electrochemical H_2O_2 production has become a hit in recent years. Two-electron oxygen reduction reaction (2-electron ORR) is the central core for the electrochemical H_2O_2 production, since it is ended with this valuable chemical: hydrogen peroxide (see equation 1)[5, 6].

$$O_2 + 2e^- + 2H^+ = H_2O_2$$

$$E_0 = 0.69 \text{ V } vs. \text{ RHE (pH < 11.6)} \qquad \text{Equation (1)}$$

Catalysts with efficient 2-electron ORR activity are urgently to explore for decentralized H_2O_2 production. According to DFT calculation, catalysts with moderate absorption energy of *OOH oxygenated intermediate at the top of Sabatier volcano plot have the highest 2-electron ORR activity[7, 8]. Noble metals such as Pd, Au and Pt with the absorption energy of *OOH located near the top of the volcano plots have been suggested to be excellent 2-electron ORR catalysts[9]. Unfortunately, the expensiveness and scarcity in nature of noble metals hinder their large-scale application[10, 11]. Carbon materials have emerged as the most possible candidates to replace noble metals due to its low price and high catalytic activity towards 2-electron ORR[12-16]. Compared to noble metals, carbon materials have an oxygen adsorption energy located at the weak bonding brunch in volcano plots, which is favorable for H_2O_2 desorption[17].

Perfect carbon materials always have low ORR activity due to the inert carbon surface. Heteroatomic doping is an effective strategy to activate carbon surface by causing charge

Received 24 February 2021; accepted 1 March 2021

① Supported by the Science and Technology Planning Project of Fujian Province (2018J01023) and the STS Project of Fujian Province (2018T 3024)

② Corresponding authors. Xu Jiao-Xing (E-mail: xujx_1220@fjirsm.ac.cn) and Guan Lun-Hui (E-mail: guanlh@fjirsm.ac.cn)

and spin re-distributions on graphene hexagon frameworks, which facilitate the oxygen absorption, activation and product desorption[18, 19]. Nonmetal elements like nitrogen, sulfur and halogens have been found to be "active" to promote ORR activities[20-22]. However, most of them are reported to favor 4-electron ORR preferably. Recently, Cui et al and McCloskey et al reported that oxidized multi-walled carbon nanotubes or graphene can act as potential 2-electron ORR catalysts[23, 24]. Single-walled carbon nanotube (SWNT), the most conductive member in carbon family, is a potential candidate deserved to be explored. Nevertheless, the traditional Hummer's method is so intensive to tear SWNT into graphene pieces, destroying the highly conductive tube structure[25]. Therefore, the search of oxidative media for easily scalable and mild oxidation of SWNT is highly desirable and the oxygenated defect-driven catalytic active site for 2-electron ORR needed to be further understood.

In this work, we present a selective and efficient nonprecious electrocatalyst based on single-walled carbon nanotubes (SWNTs), prepared through an easily scalable mild oxidation with different oxidative acids including sulfur acid, nitride acid and mixed sulfur/nitride acids, respectively. The highly oxidized SWNT treated by mixed acids exhibits the best activity and selectivity of electroreduction of oxygen to synthesize H_2O_2 at low overpotential in alkaline and neutral media. Spectroscopic characterizations suggested that the C–O is vital for catalyzing 2-electron ORR, providing an insightful understanding of defected carbon surface as the active catalytic sites for 2-electron ORR.

2 EXPERIMENTAL

2. 1 Experiments and methods

SWNTs purification The commercial Tuball SWNTs (OCSIAL company) contain some metal catalysts for growth. For purification, 500 mg SWNT was ultrasonicately dispersed and refluxed in diluted H_2O_2 solution (4.9 mol L^{-1}) at 140 ^oC for 3 h. Then one half (75 mL) of the solution was decanted and the same volume of concentrated hydrochloric acid was added for refluxing for another 3 h. After that, the purified SWNTs (P-SWNTs) were washed with distilled water for at least five times under filtration and vacuum dried at 80 ^oC overnight.

Surface oxidation of SWNTs In parallel, the oxidation of SWNTs was carried out in concentrated nitric acid, sulfuric acid and mixed nitric acid/sulfuric acid (volume ratio = 1:3) respectively under refluxing in a 70 ^oC oil bath for 2 h. The products were filtered and washed with water and ethanol until the residue pH value was neutral, and then dried overnight at 80 ^oC. The obtained sample was named as O-SWNT-NA, O-SWNT-SA and O-SWNT-SA/NA correspondingly.

2. 2 Physical characterizations

X-ray powder diffraction spectroscopy (XRD) was recorded on Rigaku miniflex600 with Cu*Ka* radiation (0.154 nm) with a scan rate of 2 ^{o}/min. Raman spectra were performed in a Horiba Jobin Yvon LabRAM ARAMIS system equipped with the 532 nm as the light source. All the recorded spectra were normalized by their maximum value of G bands[26]. The transmission electron microscopic (TEM) images were recorded on a JEOL JEM-2100F microscope with the acceleration voltage of 200 kV. X-ray photoelectron spectroscopy (XPS) was performed on ESCALAB 250 Xi. All the peaks were calibrated to the amorphous C–C peak (284.8 eV)[27], and normalized to their corresponding highest C1*s* peaks.

2. 3 Electrochemical measurement

The homogeneous ink was prepared by sonicately blending the mixture of 1 mg catalyst, 0.54 mL isopropanol and 0.06 mL nafion solution (5 wt%) for 3 h at room temperature. Then 6 uL ink was coated drop by drop on the glassy carbon disk with geometric area of 0.237 cm^2 on a rotating ring disk electrode (RRDE) and used as a working electrode. The KCl-saturated Ag/AgCl electrode and graphite rod were used as the reference and counter electrodes. Linear sweep voltammetric (LSV) measurement and cyclic voltammetric (CV) measurement were recorded on a CHI 760D electrochemical workstation coupling with the above RRDE technique. Before LSV tests, 60 segments of CV in the potential range of 1~0 V (*vs*. reversible hydrogen electrode, RHE) was applied to stabilize the catalyst layer. Then LSV curves at the rotating speed of 1600 rpm were recorded in O_2-saturated 0.1 M KOH, 0.1 M K_2SO_4 and 0.1 M $HClO_4$, with a scan rate of 5 mV s^{-1}. The platinum ring electrode was biased at 1.2 V (*vs*. RHE) during the LSV tests in order to fully oxidize the H_2O_2 nearby. In addition, LSV curves were

also recorded in N_2-saturated electrolyte as background subtraction to eliminate the double-layer electric influences. The selectivity towards 2-electron ORR was calculated by:

$$H_2O_2\% = 200 \times I_R/(I_D \times N_c + I_R)$$

where the I_R, I_D and N_c (0.38) are the ring current, disk current and collection efficiency.

The J_K was calculated by: $1/J = 1/J_L + 1/J_K$

$$J_L = 0.2nFC_oD_o^{2/3}\nu^{-1/6}\omega^{1/2}$$

Where the n, F, C_o, D_o, ν and ω represent the transfer electron, faraday constant (96485 C mol^{-1}), bulk oxygen concentration (1.3 mM), diffusion coefficient (1.9 × 10^{-5} cm^2 s^{-1}) and kinematic viscosity (0.01 cm^2 s^{-1}) of the solution and angular velocity, respectively.

3 RESULTS AND DISCUSSION

3. 1 Synthesis and characterization

As schematically illustrated in Fig. 1a, the surface oxidation degree of SWNTs can be tailored by varying the oxidative acids. The mono sulfuric acid or nitric acid has moderate ability to oxidize the SWNT. While the mixed sulfur and nitric acid with aqua regia-like features is highly oxidative to SWNT, which is proved by the oxygen analysis in samples. As estimated from the X-ray photoelectron survey spectra in Fig. S1, the O-SWNT-SA/NA has the highest oxygen content of 10.9 at.%, nearly twice as the oxygen contents of O-SWNT-SA (6.08 at.%) and O-SWNT-NA (7.5 at.%). Raman spectroscopy has been widely used to characterize SWNT for the unique one-dimensional and electronic structures[25]. In a full Raman spectrum, the typical SWNT has the radical breathing mode (RBM), D/2D mode and G mode[28]. The RBM peaks located around 150 cm^{-1} are important indicators for the diameters of SWNTs, in which a higher wavenumber of RBM corresponds to the SWNT with relative smaller diameters according to Eq. 2[29].

$$RBM = A/d_t + B$$

Where the A and B parameters are determined experimentally, and d_t is the diameter of SWNT. All the normalized RBM peaks of oxidized SWNTs and the referred purified SWNT (P-SWNT) are shown in Fig. 1b. As can be seen, the intensities of the RBM peaks tend to gradually decrease from P-SWNT to O-SWNT-SA/NA, and the O-SWNT-SA/NA exhibits the lowest intensity of RBM in four samples, proving the existence of high oxygen contents, which diminishes the SWNT characteristic Raman RBM peaks. More interestingly, the oxidized SWNTs demonstrated much weaker RBM at the right side of higher wavenumber (~175 cm^{-1}) than those of P-SWNT, indicating the SWNTs (around 175 cm^{-1}) with smaller diameters are more susceptible to the acidic oxidation. D modes are characteristics from defects such as carbon empty and doped heteroatoms[30]. In Fig. 1c, the ratios of I_D/I_G increase correspondingly with the oxygen contents for the P-SWNT to O-SWNT-SA/NA, indicating the successful oxidation of SWNT and controlling of the defects concentration by varying oxidative acids. Furthermore, the G modes of the oxidized SWNTs (Fig. 1d) show significant peak-shifts towards higher wavenumber compared to P-SWNT, implying the *p*-doping occurred by hanging with oxygen-containing groups on SWNT[31, 32]. Benefited from the highest oxygen contents, the O-SWNT-SA/NA exhibits the largest peak-shift in three oxidized SWNTs. Such electronic doping can alter the local electronic density of carbon surface, and thus can facilitate the absorption, activation or desorption of product during ORR[14]. Here, it should be noted that the acidic oxidation did not tear open the graphitized walls of SWNTs, as proved by the well-retained typical (10) peaks of SWNT in XRD patterns (Fig. 1e). The (10) peaks result from the oriented stacking of single SWNTs[33, 34], called SWNT bundles. TEM observation in Fig. 1f confirmed no obviously detached graphitic fragments, suggesting the oxidation methods by mono or mixed acids are relatively mild compared to Hummer's method[35, 36]. The well-preserved SWNT structures might guarantee the feasible conductivity and electrochemical charge transfer between SWNTs and absorbed oxygen molecules for ORR.

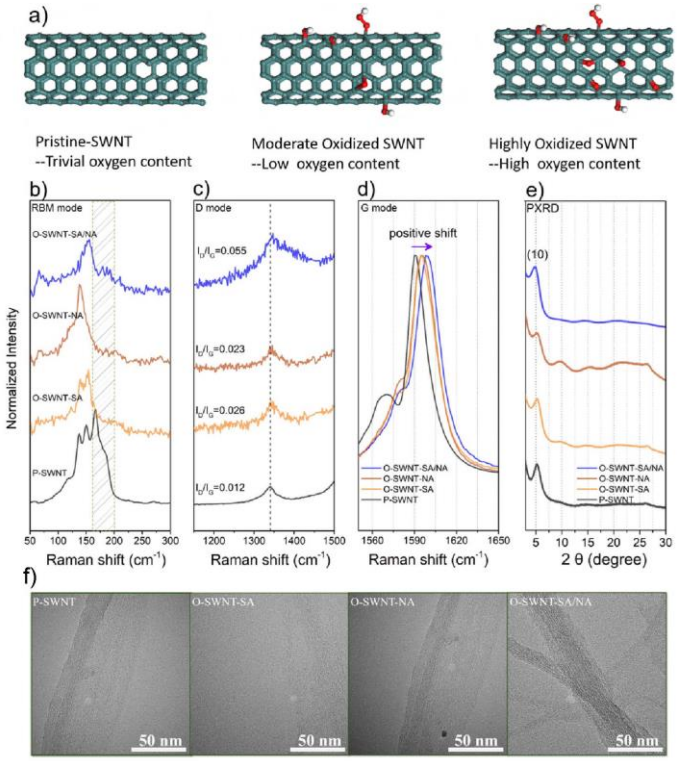

Fig. 1. a) Schematic illustration of the surface oxidation degree of SWNT, and b) RBM mode, c) D mode, d) G mode and e) XRD patterns and f) TEM images of P-SWNT, O-SWNT-SA, O-SWNT-NA and O-SWNT-SA/NA

3. 2 Electrochemistry

Linear sweep voltammetry (LSV) was employed to evaluate the ORR performances of the P-SWNT and O-SWNT samples. Fig. 2a-b shows the LSV curves (including disk and ring currents) in alkaline media (0.1 M KOH). In terms of onset potential, the ORR activities of P-SWNT and oxidized SWNT follow a clear order of O-SWNT-SA/NA > O-SWNT-NA > O-SWNT-SA > P-SWNT. The P-SWNT has relative low selectivity (< 70%) towards 2-electron ORR, especially at low potential range, which agrees with previous reports[37]. With the increase of oxygen contents by acidic treating, the catalytic 2-electron ORR selectivity improves considerably, and reaches a high level of 80~90% for O-SWNT-SA/NA, which implies the important role of introducing oxygen-containing groups on carbon surface to regulate 2-electron ORR processes. Since O-SWNT-SA/NA has the highest oxygen content, it demonstrates the best 2-electron ORR activity and selectivity. Similarly, the P-SWNT and oxidized samples show the same order of catalytic activity in neutral media (0.1 M K_2SO_4), as displayed in Fig. 2c-d. More importantly, the high 2-electron ORR selectivity performed in neutral electrolyte is more valuable for application than in alkaline, because the hydrogen peroxide tends to easily self-decompose in alkaline solution (pH > 11.6). Therefore, the O-SWNT-SA/NA catalyst has an optimized activity and selectivity (85~90%) owing to the enriched oxygen-containing groups hung on the tube structure of SWNTs.

As the best 2-electron ORR catalyst, the pH-dependent ORR properties of O-SWNT-SA/NA were also investigated, as shown in Fig. 2e. From the kinetic regions in LSV data, the onset potentials decrease with 0.059 V (vs RHE) per pH from alkaline media (0.1 M KOH) to acidic media (0.1 M $HClO_4$). No apparent overpotential was observed in alkaline media (pH = 13), which reaches nearly 1.0 V at pH = 1. This observation is ascribed to the fact that ORR proceeds via the non-coupled proton-electron transfer[38]. The Tafel plots of O-SWNT-SA/NA (Fig. 2c) at different media are re-plotted according to the LSV data. It is seen that the Tafel slopes in alkaline (63 mV dec^{-1} for pH 13) and neutral (71 mV dec^{-1} for pH 7) media are much smaller than that in acidic media (169 mV dec^{-1} for pH 1). Therefore, O-SWNT-SA/NA shows more rapid kinetics of 2-electron ORR under alkaline and neutral electrolytes.

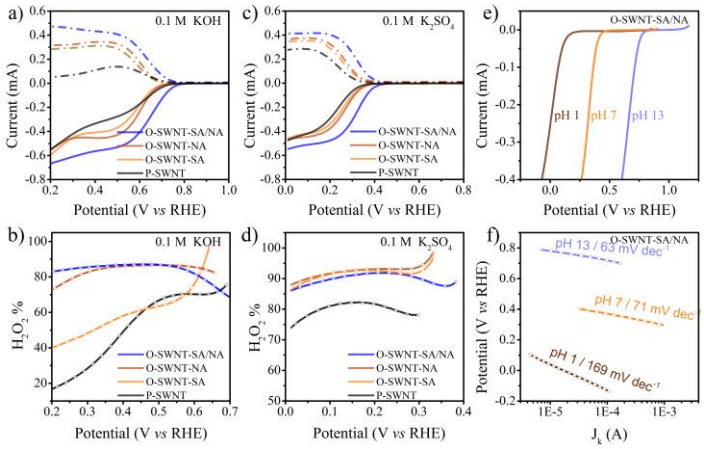

Fig. 2. Oxygen reduction performance of P-SWNT, O-SWNT-SA, O-SWNT-NA and O-SWNT-SA/NA. a) and c) LSV curves at 1,600 rpm (solid lines) and simultaneous H_2O_2 detection currents at the ring electrode (dashed lines) in 0.1 M KOH and 0.1 M K_2SO_4; b) and d) the corresponding 2-electron selectivity; e) pH-dependence of polarized curves of O-SWNT-SA/NA and f) the Tafel plots

To further understand the underlying mechanisms of enhanced ORR selectivity of oxidized SWNTs, according to the previous-reported work[39], XPS-O1*s* spectra can be deconvoluted into two oxygen species: the C–O and C=O, their relative contents are recorded in Fig. 3a and Table S1. As displayed in Fig. 3, the C–O content linearly increases in the order of P-SWNT < O-SWNT-SA < O-SWNT-NA < O-SWNT-SA/NA, while the C=O content keeps almost unchanged in the four samples. The correlation of the contents of C–O, C=O and 2-electron ORR activity and selectivity at 0.3 V (0.1 M KOH) is plotted in Fig. 3b. Obviously, the positive dependence of the selectivity and the activity with the atomic contents of C–O is observed, indicating the vital roles of C–O in regulating the activity and selectivity of 2-electron ORR.

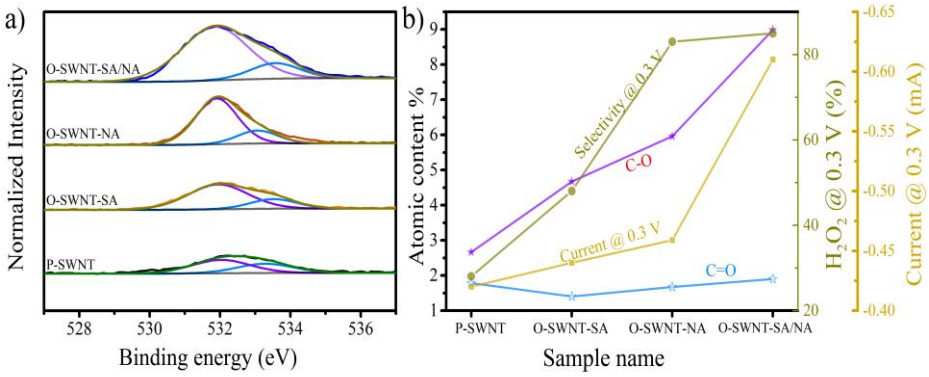

Fig. 3. a) XPS-O1S spectra of P-SWNT, O-SWNT-SA, O-SWNT-NA and O-SWNT-SA/NA. b) Plot of the C-O (purple), C=O (blue), selectivity at 0.3 V (0.1 M KOH)(green) and current at 0.3 V (0.1 M KOH) (yellow)

4 CONCLUSION

In summary, we have developed an easy and mild oxidation method to activate the surface of the SWNT and tailored the oxygen contents with three types of acids. Electrochemical tests proved that the most oxidized SWNT can exhibit efficient 2-electron ORR performance, and pointed a potential application in neutral electrolyte for electrochemical production of hydrogen peroxide. By employing spectroscopic characterizations, it is observable that there were charge transfers occurring after surface oxidation by different acids and a strong dependence of the 2-electron ORR activity with the C–O content. Combining with the composition and structural characterizations, we tentatively proposed that the C–O is important for the 2-electron ORR. This work provides an insightful understanding of the important role of C–O in 2-electron ORR, and gives a potential guidance for carbon electrocatalyst design.

REFERENCES

(1) Xia, C.; Xia, Y.; Zhu, P.; Fan, L.; Wang, H. Direct electrosynthesis of pure aqueous H_2O_2 solutions up to 20% by weight using a solid electrolyte. *Science* **2019**, 366, 226–231.

(2) Jiang, K.; Zhao, J.; Wang, H. Catalyst design for electrochemical oxygen reduction toward hydrogen peroxide. *Adv. Funct. Mater.* **2020**, 30, 2003321.

(3) Ciriminna, R.; Albanese, L.; Meneguzzo, F.; Pagliaro, M. Hydrogen peroxide: a key chemical for today's sustainable development. *Chemsuschem.* **2016**, 9, 3374–3381.

(4) Campos-Martin, J. M., Blanco-Brieva, G., Fierro, J. L. Hydrogen peroxide synthesis: an outlook beyond the anthraquinone process. *Angew. Chem. Int. Ed.* **2006**, 45, 6962–6984.

(5) Yang, S.; Verdaguer-Casadevall, A.; Arnarson, L.; Silvioli, L.; Čolić, V.; Frydendal, R.; Rossmeisl, J.; Chorkendorff, I.; Stephens, I. E. L. Toward the decentralized electrochemical production of H_2O_2: a focus on the catalysis. *ACS Catalysis* **2018**, 8, 4064–4081.

(6) Siahrostami, S.; Villegas, S. J.; Bagherzadeh Mostaghimi, A. H.; Back, S.; Farimani, A. B.; Wang, H. Persson, K. A.; Montoya, J. A review on challenges and successes in atomic-scale design of catalysts for electrochemical synthesis of hydrogen peroxide. *ACS Catalysis* **2020**, 10, 7495–7511.

(7) Stamenkovic, V.; Mun, B. S.; Mayrhofer, K. J. J.; Ross, P. N.; Markovic, N. M.; Rossmeisl, J.; Greeley, J.; Nørskov, J. K. Changing the activity of electrocatalysts for oxygen reduction by tuning the surface electronic structure. *Angew. Chem. Int. Ed.* **2006**, 45, 2897–2901.

(8) Viswanathan, V.; Hansen, H. A.; Rossmeisl, J.; Nørskov, J. K.; Unifying the $2e^-$ and $4e^-$ reduction of oxygen on metal surfaces. *J. Phys. Chem. Lett.* **2012**, 3, 2948–2951.

(9) Siahrostami, S.; Verdaguer-Casadevall, A.; Karamad, M.; Deiana, D.; Malacrida, P.; Wickman, B.; Escudero-Escribano, M.; Paoli, E. A.; Frydendal, R.; Hansen, T. W.; Chorkendorff, I.; Stephens, I. E. L.; Rossmeisl, J. Enabling direct H_2O_2 production through rational electrocatalyst design. *Nature Mater.* **2013**, 12, 1137–1143.

(10) Verdaguer, C. A.; Deiana, D.; Karamad, M.; Siahrostami, S.; Malacrida, P.; Hansen, T. W.; Rossmeisl, J.; Chorkendorff, I.; Stephens, I. E. L. Trends in the electrochemical synthesis of H_2O_2: enhancing activity and selectivity by electrocatalytic site engineering. *Nano Lett.* **2014**, 14, 1603–1608.

(11) Shen, R.; Chen, W.; Peng, Q.; Lu, S.; Zheng, L.; Cao, X.; Wang, Y.; Zhu, W.; Zhang, J.; Zhuang, Z.; Chen, C.; Wang, D.; Li, Y. High-concentration single atomic Pt sites on hollow CuS_x for selective O_2 reduction to H_2O_2 in acid solution. *Chem.* **2019**, 5, 2099–2110.

(12) Pang, Y.; Wang, K.; Xie, H.; Sun, Y.; Titirici, M. M.; Chai, G. L. Mesoporous carbon hollow spheres as efficient electrocatalysts for oxygen reduction to hydrogen peroxide in neutral electrolytes. *ACS Catalysis* **2020**, 10, 7434–7442

(13) Zhang, J.; Zhang, G.; Jin, S.; Zhou, Y.; Ji, Q.; Lan, H.; Liu, H.; Qu, J. Graphitic N in nitrogen-doped carbon promotes hydrogen peroxide synthesis from electrocatalytic oxygen reduction. *Carbon* **2020**, 163, 154–161.

(14) Chen, S.; Chen, Z.; Siahrostami, S.; Kim, T. R.; Nordlund, D.; Sokaras, D.; Nowak, S.; To, J. W.; Higgins, D.; Sinclair, R. Defective carbon-based materials for the electrochemical synthesis of hydrogen peroxide. *ACS Sustain. Chem., Eng.* **2018**, 6, 311–317.

(15) Yuan, K.; Luetzenkirchen, H. D.; Li, L. B.; Shuai, L.; Li, Y. Z.; Cao, R.; Qiu, M.; Zhuang, X. D.; Leung, M. K. H.; Chen, Y. W.; Scherf, U. Boosting oxygen reduction of single iron active sites via geometric and electronic engineering: nitrogen and phosphorus dual coordination. *J. Am. Chem. Soc.* **2020**, 142, 2404–2412.

(16) Tang, C.; Jiao, Y.; Shi, B. Y.; Liu, J. N.; Xie, Z. H.; Chen, X.; Zhang, Q. Coordination tunes selectivity: two-electron oxygen reduction on high-loading molybdenum single-atom catalysts. *Angew. Chem. Int. Ed.* **2020**, 59, 9171–9176.

(17) Kulkarni, A.; Siahrostami, S.; Patel, A.; Nørskov, J. K. Understanding catalytic activity trends in the oxygen reduction reaction. *Chem. Rev.* **2018**, 118, 2302–2312.

(18) Feng, X.; Bai, Y.; Liu, M.; Li, Y.; Yang, H.; Wang, X.; Wu, C. Untangling respective effects of heteroatom-doped carbon materials in batteries, supercapacitors and ORR to design high-performance materials. *Energy, Environ. Sci.* **2021**, DOI: 10.1039/D1EE00166C.

(19) Gong, K.; Du, F.; Xia, Z.; Durstock, M.; Dai, L. Nitrogen-doped carbon nanotube arrays with high electrocatalytic activity for oxygen reduction. *Science* **2009**, 323, 760–764.

(20) Liu, X.; Dai, L. Carbon-based metal-free catalysts. *Nature Rev. Mater.* **2016**, 1, 16064.

(21) Perazzolo, V.; Durante, C.; Pilot, R.; Paduano, A.; Zheng, J.; Rizzi, G. A.; Martucci, A.; Granozzi, G.; Gennaro, A. Nitrogen and sulfur doped mesoporous carbon as metal-free electrocatalysts for the in situ production of hydrogen peroxide. *Carbon* **2015**, 95, 949–963.

(22) Jia, N.; Yang, T.; Shi, S.; Chen, X.; An, Z.; Chen, Y.; Yin, S.; Chen, P. N,F-Codoped carbon nanocages: an efficient electrocatalyst for hydrogen peroxide electroproduction in alkaline and acidic solutions. *ACS Sustain. Chem., Eng.* **2020**, 8, 2883–2891.

(23) Lu, Z.; Chen, G.; Siahrostami, S.; Chen, Z.; Liu, K.; Xie, J.; Liao, L.; Wu, T.; Lin, D.; Liu, Y.; Jaramillo, T. F.; Nørskov, J. K.; Cui, Y. High-efficiency oxygen reduction to hydrogen peroxide catalysed by oxidized carbon materials. *Nature Catal.* **2018**, 1, 156–162.

(24) Kim, H. W.; Ross, M. B.; Kornienko, N.; Zhang, L.; Guo, J.; Yang, P.; McCloskey, B. D. Efficient hydrogen peroxide generation using reduced graphene oxide-based oxygen reduction electrocatalysts. *Nat. Catal.* **2018**, 1, 282–290.

(25) Kosynkin, D. V.; Higginbotham, A. L.; Sinitskii, A. L.; Jay R.; Dimiev, A. P. B.; Katherine, T.; James, M. Longitudinal unzipping of carbon nanotubes to form graphene nanoribbons. *Nature* **2009**, 458, 872–U5.

(26) Hu, R. T.; Wu, C. X.; Hou, K.; Xia, C.; Yang, J.; Guan, L. H.; Li, Y. Tailoring the electrocatalytic oxygen reduction reaction pathway by tuning the electronic states of single-walled carbon nanotubes. *Carbon* **2019**, 147, 35–42.

(27) Briggs, D.; Fairley, N. XPS of chemically modified low-density polyethylene surfaces: observations on curve-fitting the C 1s spectrum. *Surf. Interface Anal.* **2002**, 33, 283–290.

(28) Kharlamova, M. V. Advances in tailoring the electronic properties of single-walled carbon nanotubes. *Prog. Mater. Sci.* **2016**, 77, 125–211.

(29) Fantini, C.; Jorio, A.; Souza, M.; Strano, M. S.; Dresselhaus, M. S.; Pimenta, M. A. Optical transition energies for carbon nanotubes from resonant Raman spectroscopy: environment and temperature effects. *Phy. Rev. Lett.* **2004**, 93, 147406.

(30) Brown, S. D. M.; Jorio, A.; Dresselhaus, M. S.; Dresselhaus, G. Observations of the D-band feature in the Raman spectra of carbon nanotubes. *Phys. Rev. B* **2001**, 64, 073403.

(31) Bachilo, S. M.; Strano, M. S.; Kittrell, C.; Hauge, R. H.; Smalley, R. E.; Weisman, R. B. Structure-assigned optical spectra of single-walled carbon nanotubes. *Science* **2002**, 298, 2362–2365.

(32) Wang, Y.; Liu, D.; Zhang, H.; Wang, J.; Du, R.; Li, T. T.; Qian, J.; Hu, Y.; Huang, S. Methylation-induced reversible metallic-semiconducting transition of single-walled carbon nanotube arrays for high-performance field-effect transistors. *Nano Lett.* **2020**, 20, 496–501.

(33) Jorio, A.; Souza Filho, A. G.; Dresselhaus, G.; Dresselhaus, M. S.; Swan, A. K.; Ünlü, M. S.; Goldberg, B. B.; Pimenta, M. A.; Hafner, J. H.; Lieber, C. M.; Saito, R. G-band resonant Raman study of 62 isolated single-wall carbon nanotubes. *Phys. Rev. B* **2002**, 65, 155412.

(34) Maniwa, Y.; Fujiwara, R.; Kira, H.; Tou, H.; Kataura, H.; Suzuki, S.; Achiba, Y.; Nishibori, E.; Takata, M.; Sakata, M.; Fujiwara, A.; Suematsu, H. Thermal expansion of single-walled carbon nanotube (SWNT) bundles: X-ray diffraction studies. *Phys. Rev. B* **2001**, 64, 241402.

(35) Kawasaki, S.; Matsuoka, Y.; Yokomae, T.; Nojima, Y.; Okino, F.; Touhara, H.; Kataura, H. XRD and TEM study of high pressure treated single-walled carbon nanotubes and C60-peapods. *Carbon* **2005**, 43, 37–45.

(36) Chen, J.; Yao, B.; Li, C.; Shi, G. An improved Hummers method for eco-friendly synthesis of graphene oxide. *Carbon* **2013**, 64, 225–229.

(37) Chen, C.; Zhang, X.; Zhou, Z. Y.; Yang, X. D.; Zhang, X. S.; Sun, S. G. Highly active Fe, N co-doped graphene nanoribbon/carbon nanotube composite catalyst for oxygen reduction reaction. *Electrochim. Acta* **2016**, 222, 1922–1930.

(38) Kim, H. W.; Bukas, V. J.; Park, H.; Park, S.; Diederichsen, K. M.; Lim, J.; Cho, Y. H.; Kim, J.; Kim, W.; Han, T. H.; Voss, J.; Luntz, A. C.; McCloskey, B. D. Mechanisms of two-electron and four-electron electrochemical oxygen reduction reactions at nitrogen-doped reduced graphene oxide. *ACS Catal.* **2019**, 10, 852–863.

(39) Kundu, S.; Wang, Y.; Xia, W.; Muhler, M. Thermal stability and reducibility of oxygen-containing functional groups on multiwalled carbon nanotube surfaces: a quantitative high-resolution xps and tpd/tpr study. *J. Phys. Chem. C* **2008**, 112, 16869–16878.